

Pocket resonances in low-energy antineutrons reactions with nuclei

Teck-Ghee Lee^{1*}

¹*Department of Physics, Auburn University, Auburn, Alabama 36849, USA.*

Orhan Bayrak^{2†}

²*Department of Physics, Akdeniz University, Antalya, Turkey*

Cheuk-Yin Wong^{3‡}

³*Physics Division, Oak Ridge National Laboratory^d, Oak Ridge, Tennessee 37831, USA.*

Upon investigating whether the antineutron-nucleus annihilation cross-sections at very low momenta p satisfy Bethe-Landau's power law of $\sigma_{\text{ann}}(p) \propto 1/p^\alpha$, we uncover unexpected regular oscillatory structures in the low antineutron energy region from 0.001 to 10 MeV, with small amplitudes and narrow periodicity in the logarithm of the antineutron energies, for large- A nuclei such as Pb and Ag. Subsequent semiclassical analyses of the S matrices reveal that these oscillations are pocket resonances that arise from quasi-bound states inside the effective potential pocket with a barrier. They are a continuation of the bound states in the continuum. Experimental observations of these pocket resonances will provide vital information on the properties of the optical model potentials and the nature of the antinucleon-nucleus reactions.

arXiv:2102.06691v2 [nucl-th] 16 May 2021

^d This manuscript has been authored in part by UT-Battelle, LLC, under contract DE-AC05-00OR22725 with the US Department of Energy (DOE). The US government retains and the publisher, by accepting the article for publication, acknowledges that the US government retains a nonexclusive, paid-up, irrevocable, worldwide license to publish or reproduce the published form of this manuscript, or allow others to do so, for US government purposes. DOE will provide public access to these results of federally sponsored research in accordance with the DOE Public Access Plan (<http://energy.gov/downloads/doe-public-access-plan>), Oak Ridge, Tennessee 37831, USA

* tgl0002@auburn.edu; tglee.physics@gmail.com

† bayrak@akdeniz.edu.tr

‡ wongc@ornl.gov

I. INTRODUCTION

One of the greatest mysteries in modern physics is the matter-antimatter asymmetry in the Universe [1]. To unravel this mystery, there has been a great deal of experimental and theoretical investigations on matter-antimatter interactions. So far, most of the obtained information centers around antiproton-nucleus ($\bar{p}A$) reactions and structures [2–14]. The corresponding information on antineutron-nucleus ($\bar{n}A$) reaction [2, 15], on the other hand, remains comparatively sparse and limited with the most recent work from the OBELIX collaboration [16, 17] at CERN. Nevertheless, the $\bar{n}A$ annihilation is essential in the process of quantifying signals from $n \rightarrow \bar{n}$ oscillations in matter [18–21], and the significant connection between the $\bar{n}A$ interaction-potential and the $n \rightarrow \bar{n}$ oscillations rates have also been examined theoretically [22–24].

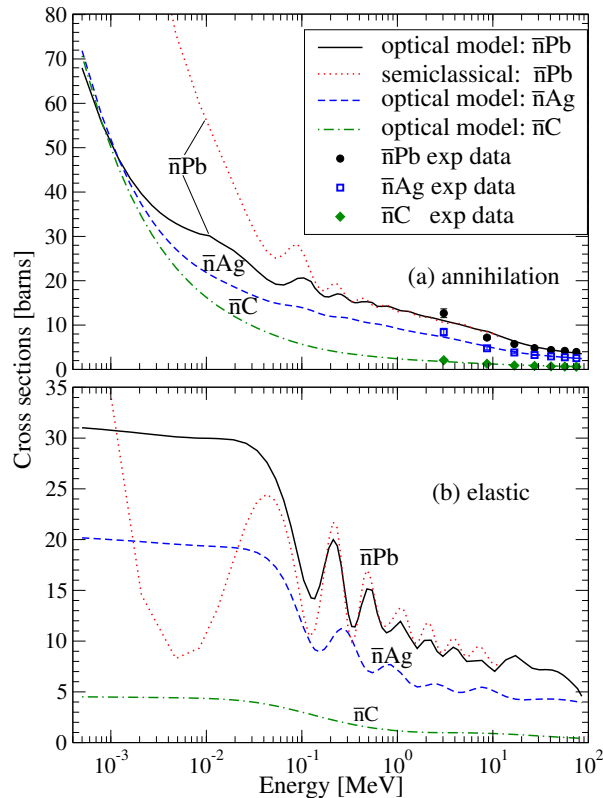


FIG. 1: Optical-model cross sections as a function of energy. (a) $\bar{n}A$ annihilation, (b) $\bar{n}A$ elastic scattering. The red dotted-curve is the semiclassical result for the $\bar{n}Pb$ reactions.

It has been generally expected that in the s -wave limit the $\bar{n}A$ and $\bar{p}A$ annihilation cross-sections are to obey Bethe-Landau’s power-law, $\sigma_{\text{ann}}^{\bar{n}A, \bar{p}A}(p) \propto 1/p^\alpha$ as a function of the antineutron momentum p , with $\alpha = 1$ for $\bar{n}A$ and $\alpha = 2$ for $\bar{p}A$ [25]. But recent experimental data (see Fig. 5 of Ref.[3]) revealed that the $\bar{n}C$ and $\bar{p}C$ annihilation cross-sections at low energies appear to follow a similar trend with only minor differences. Much curious about the puzzle, we recently introduced a new momentum-dependent optical potential to investigate the behavior of the $\bar{n}A$, and the $\bar{p}A$ annihilation cross-sections on C, Al, Fe, Cu, Ag, Sn, and Pb nuclei in the momentum range 50 to 500 MeV/ c [26], via the ECIS code [27]. The calculated results agree with the OBELIX’s annihilation cross-section data [16, 17], but the optical model calculations indicated that $\alpha \approx 1/2$ for $\bar{n}A$ and $\alpha \approx 1.5$ for $\bar{p}A$ between 40 and 100 MeV/ c , leading us to conclude that our low-energy annihilation reaction in question was yet to reach the s -wave limit.

While investigating the energy dependence of the cross-sections at even lower energies, we uncover, to our surprise, unexpected regular oscillatory structures with small amplitudes and narrow periods (in the logarithm of the energy) in the annihilation and elastic cross-sections, in the region from 0.001 to 10 MeV, as shown in Fig. 1. Such oscillations are absent for small nuclei and gain in strength as the nuclear radius increases. Its amplitude is larger for the elastic scattering than for the annihilation process. Such behavior, undoubtedly, contradicts Bethe-Landau’s power-law. It is reminiscent of a potential resonance behavior. However, the predicted oscillations appear somewhat different from that of neutron-induced total cross sections for Pb, Cd, and Ho nuclei, which arises from the Ramsauer’s resonances [28–30] that are broad potential resonances without a barrier whose peak position moves to higher energies as the

nuclear mass increases. They are also unlike those present in the high-energy $^{12}\text{C}+^{12}\text{C}$ fusion, which is due to successive addition of contributions from even values of partial waves to the identical-particle fusion cross-section, with increasing energies [31–33].

To understand the nature of these oscillations, we carry out a semiclassical S matrix analysis for $\bar{n}\text{Pb}$ reaction in which the oscillations are quite prominent. As shown in Fig. 1 the structure of the cross-section oscillations in the semiclassical calculations for $\bar{n}\text{Pb}$ agrees approximately with the structure obtained in the optical model calculations, except for the lowest energy region for which the semiclassical approximation is not applicable. We wish to show that the cross-section oscillations are physical and constitute narrow pocket resonances that can be best described as arising from quasi-bound states inside an effective potential pocket with a barrier, as depicted in Fig. 5 of Ford and Wheeler [34]. Such pocket resonances are expected to be common features of potential scattering in nuclear, atomic, molecular, and heavy-ion collisions because they are the continuation of the bound states in the continuum. They move to lower energies as the mass number of the nucleus increases as is shown in Fig. 1. To understand the origin of such resonances, a thorough analysis of the reaction process in detail is therefore needed in what follows.

II. SEMICLASSICAL ANALYSES OF THE OSCILLATIONS OF THE ANNIHILATION AND ELASTIC CROSS SECTIONS

Semiclassical descriptions of the potential scattering problem have been discussed in great details by Ford and Wheeler [34] using the Wentzel-Kramers-Brillouin (WKB) approximation, and later consolidated by other pioneering works [35–39]. However, we shall follow the Brink-Takigawa formulation [37] for complex-potential scattering that was also applied by Lee, Marty, and Ohkubo [37–39]. Accordingly, we consider the interference between a barrier

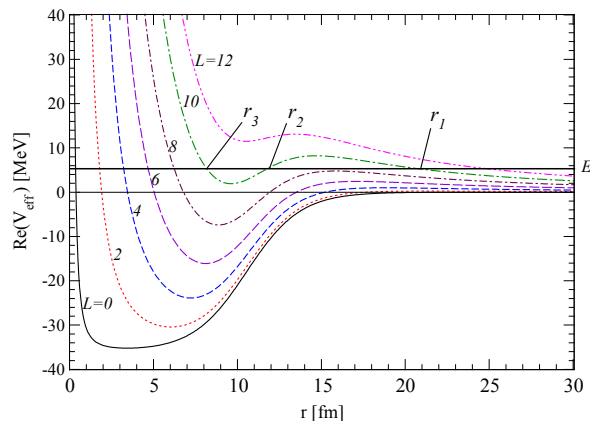


FIG. 2: Real part of the $\bar{n}\text{Pb}$ interaction potential $\text{Re}(V_{\text{eff}}(r, E))$ at a sample energy E , where only the potential curves for even orbital angular momentum L are displayed. The $r_{1,2,3}$ denote three turning points for $\text{Re}(V_{\text{eff}}(r, E))$.

wave reflected at the potential barrier and modified by the tunneling effect, and an internal wave that penetrates the barrier, into the potential pocket, and reemerges through the barrier out to $r \rightarrow \infty$.

For a given E and a partial wave L , the total phase shift $\delta = \delta(E, L)$ is related to the WKB phase function δ_{WKB} , the action phase angle δ_{ij} between the turning points r_i and r_j , tunneling phase ϕ , tunneling phase angle ξ and

tunneling coefficient w by [37–39],

$$\delta = \delta_{\text{WKB}} - \phi + \tan^{-1}\{w(\xi) \tan(\delta_{32} - \phi)\}, \quad (1)$$

$$\delta_{\text{WKB}} = \frac{\pi}{2}(L + \frac{1}{2}) - kr_1 + \int_{r_1}^{\infty} (K - k)dr, \quad (2)$$

$$\delta_{ij} = \int_{r_i}^{r_j} K dr, \quad (3)$$

$$\phi = \frac{1}{2} \left(\xi \ln(\xi/e) - \arg \Gamma\left(\frac{1}{2} + i\xi\right) \right), \quad (4)$$

$$\xi = -\frac{i}{\pi} \delta_{21}, \quad (5)$$

$$w(\xi) = \frac{\sqrt{(1 + e^{-2\pi\xi}) - 1}}{\sqrt{(1 + e^{-2\pi\xi}) + 1}}, \quad (6)$$

where $K = \sqrt{2\mu[E - V_{\text{eff}}(r, E)]/\hbar^2}$, $k = \sqrt{2\mu E/\hbar^2}$, E is the center-of-mass energy, and μ is the reduced mass of the collision pair. The turning points $r_{1,2,3}$ are the roots of $E - V_{\text{eff}}(r, E) = 0$, as displayed in Fig. 2. In our case, $V_{\text{eff}}(r, E)$ is the Langer's modified interaction potential,

$$V_{\text{eff}}(r, E) = \frac{-(V(E) + iW)}{1 + \exp\{(r - R)/a_o\}} + \frac{\hbar^2(L + 1/2)^2}{2\mu r^2}. \quad (7)$$

We adapt the same momentum-dependent optical potential used in our earlier work [26] in the present semiclassical theory. The values for the parameters $r_o = R/A^{1/3}$, a_o and volume terms $V(E)$ and W are listed in Table 1, 2, and 3 in [26]. To keep the analyses simple, we consider only the nuclear volume terms in the present semiclassical theory.

Figure 2 illustrates the real part of the potential $\text{Re}(V_{\text{eff}}(r, E))$ as a function of internuclear distance r and different L at a sample energy E for the $\bar{n}\text{Pb}$ interaction. With the nuclear potential that has a negative imaginary potential W , the turning points $r_{1,3}$ are below the real axis of the complex-plane and r_2 lies above, and the $V_{\text{eff}}(r, E)$ for a given E must be an analytic function of r . The integrands in the action phase angle δ_{ij} are multiple-valued quantities involving branch cuts. The integration paths in the complex plane need to be chosen so that the action phase angles δ_{ij} and ξ are positive, as discussed in [37].

As mentioned earlier in the Introduction, the semiclassical cross-sections for $\bar{n}\text{Pb}$ reaction give an approximate representation of the optical model results, except for the lowest energy region. Our task is to carry out a detailed semiclassical partial wave analysis to pinpoint the origin of the cross-section oscillations.

So we concentrate on the interference between the barrier waves and the internal waves and split the total S matrix element into the barrier wave contribution S_B , and the internal wave contribution S_I :

$$S = e^{2i\delta} = S_B + S_I, \quad (8)$$

$$S_B = \frac{e^{2i\delta_{\text{WKB}}}}{N}, \quad (9)$$

$$\begin{aligned} S_I &= \left[\frac{e^{2i\delta_{\text{WKB}}}}{N} \right] e^{-2\pi\xi} \left[\frac{e^{2i\delta_{32}}}{N} \right] \\ &\quad \times \left[1 + \frac{e^{2i\delta_{32}}}{N} + \left(\frac{e^{2i\delta_{32}}}{N} \right)^2 + \left(\frac{e^{2i\delta_{32}}}{N} \right)^3 + \dots \right] \\ &= \left[\frac{e^{2i\delta_{\text{WKB}}}}{N} \right] e^{-2\pi\xi} \left[\frac{e^{2i\delta_{32}}}{N} \right] \left[\frac{1}{1 + e^{2i\delta_{32}}/N} \right], \end{aligned} \quad (10)$$

where $N = \sqrt{2\pi} \exp(-2\pi\xi + i\xi \ln(\xi/e))/\Gamma(\frac{1}{2} + i\xi)$ is the barrier-penetration factor. The factor $1/(1 + e^{2i\delta_{32}}/N)$ in the S_I term is from Padé approximation, where $e^{2i\delta_{32}}/N$ is the amplitude of penetration-weighted internal-wave. Thus, the factor $e^{2i\delta_{32}}/(N + e^{2i\delta_{32}})$ essentially describes the sum of amplitudes of multiple reflections of internal-wave inside the potential pocket [37, 38]. Knowing these S -matrices, $\sigma_{\text{ann}}^{\text{tot}} = \sum_L \sigma_{\text{ann}}(L) = (\pi/k^2) \sum_L (2L + 1)(1 - |S|^2)$ and $\sigma_{\text{el}}^{\text{tot}} = \sum_L \sigma_{\text{el}}(L) = (\pi/k^2) \sum_L (2L + 1)(|1 - S|^2)$ define the cross sections for annihilation and elastic scattering, can be readily evaluated.

Partial wave analysis of the annihilation oscillations in terms of the interference of the barrier and the internal

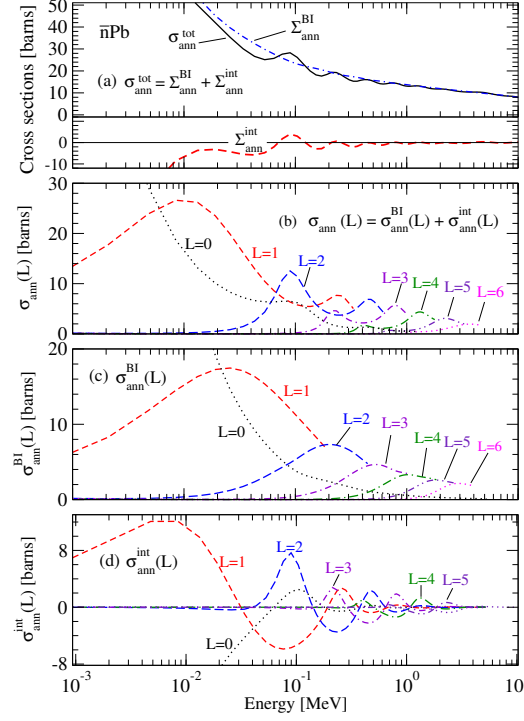


FIG. 3: Semiclassical results for $\bar{n}\text{Pb}$ annihilation as a function of energy. (a) is the total cross section of Eq.(11), (b) is the partial-wave cross section of Eq.(11), (c) is the non-interference cross section of Eq.(12) and (d) is the interference cross section of Eq.(13)

waves gives [39]

$$\sigma_{\text{ann}}^{\text{tot}} = \Sigma_{\text{ann}}^{\text{BI}} + \Sigma_{\text{ann}}^{\text{int}} = \sum_{L=0}^{\infty} (\sigma_{\text{ann}}^{\text{BI}}(L) + \sigma_{\text{ann}}^{\text{int}}(L)), \quad (11)$$

$$\sigma_{\text{ann}}^{\text{BI}}(L) = \frac{\pi}{k^2} (2L+1) (1 - |S_B|^2 - |S_I|^2), \quad (12)$$

$$\sigma_{\text{ann}}^{\text{int}}(L) = \frac{\pi}{k^2} (2L+1) (-2\text{Re}\{S_B S_I^*\}), \quad (13)$$

where $\sigma_{\text{ann}}^{\text{int}}(L)$ arises from the interference between the internal and barrier waves, and $\sigma_{\text{ann}}^{\text{BI}}(L)$ from the remaining non-interference term.

We show in Fig. 3(a) the results of the separation of the total annihilation cross section $\sigma_{\text{ann}}^{\text{tot}}$ of Eq. (11) into the non-interference part, $\Sigma_{\text{ann}}^{\text{BI}}$, and the interference part, $\Sigma_{\text{ann}}^{\text{int}}$ as a function of E . The non-interference $\Sigma_{\text{ann}}^{\text{BI}}$ produces the familiar $1/p$ -like dependence with decreasing energy without any oscillations. In contrast, the interference part $\Sigma_{\text{ann}}^{\text{int}}$ does oscillate, giving rise to the total (sum of all partial-wave) annihilation cross section $\sigma_{\text{ann}}^{\text{tot}}$ that oscillates on the smooth $1/p$ background as shown in the plot.

Figure 3(b) shows the decomposition of the total annihilation cross section, $\sigma_{\text{ann}}^{\text{tot}}$, into different partial waves contributions, $\sigma_{\text{ann}}(L)$. Except for the $L=0$ partial-wave that resembles the $1/p$ -like behavior, the other partial waves display a double peak. Fig. 3(c) shows the $\sigma_{\text{ann}}^{\text{BI}}(L)$ for different L as given by Eq.(12), indicating a monotonically decreasing cross section for $L=0$ and a single broad peak for higher partial waves.

Figure 3(d) displays $\sigma_{\text{ann}}^{\text{int}}(L)$ for different L as given by Eq.(13). Inspection of Eq.(9), (10) and (13) reveals that the oscillations of $\sigma_{\text{ann}}^{\text{int}}(L)$ are governed by $[-2\text{Re}\{S_B S_I^*\}]$ in which $[-(S_B S_I^*)]$ can be factorized into

$$-S_B S_I^* = \underbrace{\left[\frac{e^{2i\delta_{\text{WKB}}}}{N} \right]}_{\text{barrier penetration factor}} \underbrace{\left[\frac{e^{2i(\delta_{\text{WKB}} + \delta_{21})}}{N} \right]^*}_{\text{pocket factor}} \left[\frac{-e^{2i\delta_{32}/N}}{1 + e^{2i\delta_{32}/N}} \right]^*, \quad (14)$$

which depends on δ_{WKB} , δ_{21} , and δ_{32} . The real part of the above barrier penetration factor and pocket factor in Eq.(14) for various L are displayed in Fig. 4 as a function of E . In the $r_2 < r < r_1$ region below the barrier,

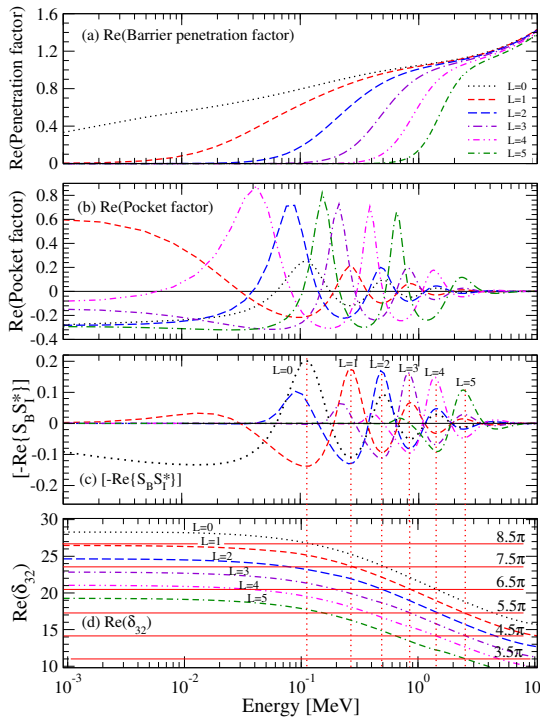


FIG. 4: For different partial waves L , the energy dependence of (a) the real part of the barrier penetration factor in Eq. (14), (b) the real part of the pocket factor in Eq. (14), (c) the quantity $[-\text{Re}\{S_B S_I^*\}]$, and (d) the quantity $\text{Re}(\delta_{32})$.

δ_{21} are predominantly imaginary, resulting in the penetration probability $\exp(2i\delta_{21}) \approx \exp(-2\pi\xi)$ with $\xi > 0$. The $(\delta_{\text{WKB}} - \delta_{\text{WKB}}^*)$ difference of the $r > r_1$ outer-most region are also predominantly imaginary, rendering $\exp[2i(\delta_{\text{WKB}} - \delta_{\text{WKB}}^*)] \approx \exp(-2\eta)$ with $\eta > 0$. We can therefore recast Eq.(13) into

$$\sigma_{\text{ann}}^{\text{int}}(L) \sim \frac{\pi}{k^2} (2L+1) |S_B| |S_I| e^{-2(\pi\xi+\eta)} [-2 \cos(2\delta_{32})]. \quad (15)$$

Consequently we find that the maxima of the annihilation cross sections $\sigma_{\text{ann}}^{\text{int}}(L)$ in Fig. 3(d) as “annihilation resonances” are located at the maxima of the real part of the pocket factor of Eq. (14) in Fig. 4(b) and the maxima of $[-\text{Re}\{S_B S_I^*\}]$ in Fig. 4(c), as marked by the vertical dashed lines in Fig. 4(c) and 4(d) for some of the resonances. Even though the barrier penetration factor of Fig. 4(a) increases approximately stepwise with increasing energy and modifies the oscillation amplitude of the pocket factor of Fig. 4(b), the final positions of the oscillation maxima as shown in Fig. 4(c) remain approximately unchanged. The maxima of the pocket factor, according to Eq.(15), occur whenever $\cos(2\delta_{32}) = -1$ (or $2\delta_{32} = (2n+1)\pi$). The subsequent maxima of $[-\text{Re}\{S_B S_I^*\}]$ are indeed located at $\delta_{32} \approx 8.5\pi, 7.5\pi$ and 4.5π , etc., respectively, as indicated by horizontal lines in Fig. 4(d). The quantity δ_{32} varies by one π unit between resonances of the same L with $\partial\delta_{32}/\partial n \approx -\pi$. We further find that wherever the horizontal lines intersect the δ_{32} curves of Fig. 4(d), each intersection point approximately, and respectively, matches each maximum of $[-\text{Re}\{S_B S_I^*\}]$ in Fig. 4(c) and each maximum of $\sigma_{\text{ann}}^{\text{int}}(L)$ in Fig. 3(d). This means that the condition for an annihilation resonance at a cross-section maximum at the energy E is

$$\delta_{32}(E, L) \approx (n_L - n'_L + \frac{1}{2})\pi, \quad (16)$$

where n_L is the number of bound and quasi-bound radial states lower than E for the angular momentum L and n'_L ($= 0, 1, 2, \dots$) is the additional resonance number above the first resonance of the same L . The above sign of n'_L in Eq. (16) depends on $\partial V/\partial E$ as a function of E .

Since $\delta_{32}(E, L)$ is the action phase angle integrating over the confining potential pocket of $V_{\text{eff}}(r, E)$, condition of Eq.(16) is just the quantization condition for a quasi-bound state inside the pocket. Thus, the “pocket resonance” is, in fact, a continuation of the bound states in the continuum trapped in a pocket with a barrier as depicted in Fig. 5 of Ford and Wheeler [34]. The condition of Eq. (16) for the resonances suggests that pocket resonances occur quite generally in potential scattering problems. Their observations however depend on the degree of absorption as we shall discuss later.

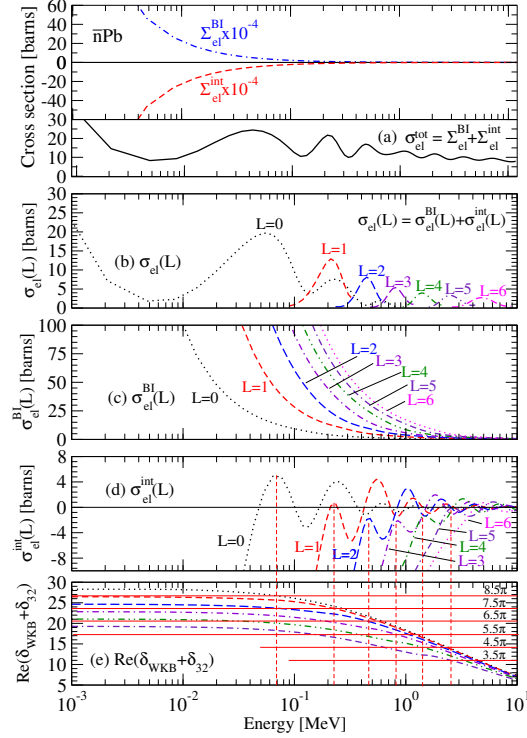


FIG. 5: Semiclassical results for $\bar{n}\text{Pb}$ elastic scattering as a function of energy. (a) is the total cross section of Eq.(17), (b) is the partial-wave cross section of Eq.(17) for different L , (c) is the non-interference cross section of Eq.(18), (d) is the interference cross section of Eq.(19) and (e) is the $\text{Re}(\delta_{\text{WKB}} + \delta_{32})$ for different L .

We now examine the elastic oscillations with

$$\sigma_{\text{el}}^{\text{tot}} = \Sigma_{\text{el}}^{\text{BI}} + \Sigma_{\text{el}}^{\text{int}} = \sum_{L=0}^{\infty} (\sigma_{\text{el}}^{\text{BI}}(L) + \sigma_{\text{el}}^{\text{int}}(L)), \quad (17)$$

$$\sigma_{\text{el}}^{\text{BI}}(L) = \frac{\pi}{k^2} (2L+1) (1 + |S_I|^2 + |S_B|^2), \quad (18)$$

$$\sigma_{\text{el}}^{\text{int}}(L) = \frac{\pi}{k^2} (2L+1) (2\text{Re}\{S_I^* S_B - S_I^* - S_B\}). \quad (19)$$

Figure 5(a) indicates that there is a significant cancellation of $\Sigma_{\text{el}}^{\text{BI}}$ by $\Sigma_{\text{el}}^{\text{int}}$, where $\Sigma_{\text{el}}^{\text{int}}$ has an oscillating behavior, resulting in an oscillating total elastic cross section $\sigma_{\text{el}}^{\text{tot}}$ as a function of energy as shown in Fig. 5(a).

Figure 5(b) shows the decomposition of the total elastic $\sigma_{\text{el}}^{\text{tot}}$ into different partial waves contributions $\sigma_{\text{el}}(L)$. Only the $L = 0$ partial wave has three, narrow, sinusoidal oscillations with decreasing amplitudes. The $L > 0$ curves, however, have only a single maximum with a similar shape. The first, broad maximum seen in $\sigma_{\text{el}}^{\text{tot}}$ near 0.05 MeV closely corresponds to the first maximum of $L = 0$ curve at the same energy. The subsequent, second maximum of $\sigma_{\text{el}}^{\text{tot}}$ that is near 0.2 MeV corresponds to the contributions from the $L = 1$ curve and the second maximum of $L = 0$ curve. Beyond the second maximum, each consecutive maximum now appears to be associated with a specific partial wave of $L = 2, 3, 4$, and so forth. Fig. 5(c) shows that $\sigma_{\text{el}}^{\text{BI}}(L)$ for different L from Eq.(18) decrease monotonically as energy increases.

Figure 5(d) is more interesting as it exhibits the oscillating $\sigma_{\text{el}}^{\text{int}}(L)$ as a function of E for different L . The oscillations are similar to those in the annihilation case. Although Eq.(19) is more complicated than Eq.(13) for the annihilation, we have found from our numerical calculations that the $[-2\text{Re}(S_I)]$ term dominates in the evaluation of $\sigma_{\text{el}}^{\text{int}}(L)$ over the energy range. Furthermore, the maximum of $\sigma_{\text{el}}^{\text{int}}(L)$ as an “elastic resonance” for various partial waves is located at the same energy as the maximum of $[-2\text{Re}(S_I)]$. The phase of S_I , according to Eq.(10), is given predominantly by $(\delta_{\text{WKB}} + \delta_{32})$. Numerical calculations of $(\delta_{\text{WKB}} + \delta_{32})$ indicate that the difference of the phases between elastic resonances is π , i.e., $\partial(\delta_{\text{WKB}} + \delta_{32})/\partial n \approx -\pi$.

Together with Fig. 5(d), the plot of 5(e) shows the condition for the elastic resonances at the energy E arising from

the pocket is

$$(\delta_{\text{WKB}} + \delta_{32})(E, L) \approx (n_L - n'_L + \frac{1}{2})\pi, \quad (20)$$

at which $\cos[2(\delta_{\text{WKB}} + \delta_{32})(E, L)] = -1$, substantiating the quantization condition for the elastic pocket resonance similar to that for the annihilation pocket resonance in Eq.(16), but with the addition of δ_{WKB} to δ_{32} . And because of this additional δ_{WKB} phase the location of the elastic pocket resonance energy E is slightly shifted from the annihilation pocket resonance energy for the same n and L .

Another interesting feature for both the annihilation and elastic resonances is that the resonance energies shift toward lower energies with increasing nuclear radius or mass, as is clear from Fig. 1(b) in comparing $\bar{n}\text{Ag}$ and $\bar{n}\text{Pb}$ elastic cross-sections. This arises because the pocket resonances are the continuation of the bound states in the continuum. Note that the opposite behavior occurs where the Ramsauer resonance shifts toward higher energies with increasing nuclear radius in the neutron total cross-section data for Cu, Cd, and Pb [40] and Ho [30] nuclei from 2 MeV to 125 MeV. The cause of the broad resonance and its shifts to higher energies have been explained by Peterson [29] and Marshak *et. al.* [30] using the concept of Ramsauer's interference [28].

As the incident energy further decreases below 0.03 MeV, we see the optical model predicted annihilation cross-sections for C, Ag, and Pb nuclei merge into one single curve. Parametrizing these curves with $\sigma_{\text{ann}}^{\bar{n}A}(p) \propto 1/p^{\alpha_{\bar{N}}}$ in this energy region (i.e., $1.0 \leq p \leq 2.0$ MeV/c), we found that $\alpha_{\bar{N}} = \partial \ln(\sigma_{\text{ann}}^{\bar{n}A}) / \partial \ln(p)$ for C, Ag and Pb nuclei to be ~ 1.0 , ~ 0.9 , and ~ 0.8 , respectively, which are surely close to Bethe-Landau's s -wave prediction of $\alpha_{\bar{n}} = 1$. On the elastic scattering at energies below 0.03 MeV, we notice that the scattering becomes isotropic and energy-independent. Consequently, the "s-wave" cross-section is purely geometrical effect and a constant, which can be described by a black-nucleus model with $\sigma_{\text{el}}^{\text{tot}} = \pi R^2$ [41].

It is important to point out the sensitivity of the pocket resonances on the optical model parameters W , V , and R of Eq. (7). For the pocket resonances to exist, the lifetime of the incident particle inside the potential pocket, $\hbar/2W$, must be longer than the passage time for the particle to traverse from the entrance to the exit in the pocket, of order $2R/v$, where v is the particle velocity in the pocket. This corresponds to the requirement of W to be approximately less than $W_o \sim \hbar\sqrt{2(E + |V|)/m_{\bar{n}}}/4R$. For the $\bar{n}\text{Pb}$ reaction, $W_o \sim 2.3$ MeV (estimated) for potential parameters extrapolated to the pocket resonance energy region.

The available $\bar{n}\text{Pb}$ annihilation cross-section data are consistent with the value of $W = 2.8$ MeV [26], which is comparable to the above estimate of onset value W_o . Hence, the pocket resonances are slightly diminished in oscillatory magnitudes but remain to be present for the $\bar{n}\text{Pb}$ reaction in extrapolation, as shown in Fig. 1. Other choices of W and radius parameter would not lead to a good description of the experimental annihilation data. The oscillatory amplitudes of pocket resonances will be much sharper for very small values of W but decrease as W increases, and the oscillatory pocket resonances will be absent if W is substantially large.

It has been known from the works of Brink and Takigawa [37, 38] that there is an anomalous large-angle scattering (ALAS) elastic scattering that is sensitive to the imaginary part W of the optical potential. The elastic scattering at large angles at a pocket resonance requires the passage of the incident particle from the entrance to the exit of the pocket and is likewise sensitive to the degree of absorption represented by W . We find that as a pocket resonance is associated with a specific angular momentum L which shows up as a dip in a particular angle in the elastic angular distribution at large angles, the shape of the dip, and the swing of the angular distribution at larger scattering angles is sensitively affected by the strength of W . There is also the ALAS phenomenon associated with the pocket resonance as energy is varied across the resonances energy region, similar to the other ALAS observed in Ref.[37, 38].

III. CONCLUSIONS

Optical-model calculations show oscillatory structures in $\bar{n}A$ annihilation and elastic cross-sections in the low \bar{n} energy range 0.001 to 10 MeV. The cross-sections oscillate in the logarithm of the antineutron energies with small amplitudes and narrow periods for large nuclei. This surprising behavior contradicts the generally expected Bethe-Landau's power-law in the s -wave limit.

Semiclassical S -matrix analysis provides new insight into the nature and the origin of the oscillations. Two important contributions to the structures in the reaction cross sections are found: (1) For annihilation and elastic scattering, the oscillations are attributed to the interference between the internal and barrier waves, while their smooth, $1/p$, backgrounds are mainly due to the non-interference term. (2) Delving deeper into the interference term for both reactions, we identified the maxima of the cross-sections as resonances occurred within the potential pocket. The condition for an annihilation resonance is the quantization rule: $\delta_{32}(E, L) \approx (n_L - n'_L + 1/2)\pi$, and for an elastic resonance: $(\delta_{\text{WKB}} + \delta_{32})(E, L) \approx (n_L - n'_L + 1/2)\pi$ where n_L is the the number of bound and quasi-bound radial states in the pocket below E for the partial wave L , and n'_L is the additional resonance number. So the existence of resonances is connected to the potential pocket and barrier that depends sensitively on optical potential parameters.

Experimental observations of these pocket resonances, if they occur, will provide valuable information on the properties of the optical model potentials and the nature of the reaction process. While here we have focused on $\bar{n}A$ reactions, similar potential pocket resonances are also expected for reactions involving the use of an optical potential in nuclear, atomic, molecular, and heavy-ion collisions such as in $^{12}\text{C}+^{12}\text{C}$ reactions [42], which is an important reactions in nuclear astrophysics.

ACKNOWLEDGMENT

CYW's research is supported in part by the Division of Nuclear Physics, U.S. Department of Energy under Contract DE-AC05-00OR22725.

-
- [1] A. D. Sakharov, JETP. Lett. **5** 24 (1967).
 - [2] J-M. Richard., Front. Phys. **8**, 1 (2020).
 - [3] H.Aghai-Khozani *et al.*, Nucl. Phys. A **970**, 366 (2018); Hyperfine Interact. **234**, 85 (2015); Hyperfine Interact. **229**, 31 (2014).
 - [4] S. Maury, (for the AD Team), *the Antiproton Decelerator (AD)*, CERN/PS 99-50 (HP) (1999).
 - [5] *FAIR - Facility for Antiproton and Ion Research*, Green Paper, October 2009.
 - [6] A. Bianconi, *et al.*, Phys. Lett. B **704** 461 (2011); A. Bianconi, *et al.*, Phys. Lett. B **481**, 194 (2000); A. Bianconi, *et al.*, Phys. Lett. B **492**, 254 (2000).
 - [7] F. Balestra, *et al.*, Phys. Lett. B **230**, 36 (1989); F. Balestra, *et al.*, Nucl. Phys. A **452**, 573 (1986); F. Balestra, *et al.*, Phys. Lett. B **165**, 265 (1985); F. Balestra, *et al.*, Phys. Lett. B **149**, 69 (1984).
 - [8] E. Klempt, C. Batty and J.-M. Richard, Phys. Rep. **413**, 197 (2005).
 - [9] A. Gal, E. Friedman, and C. J. Batty, Phys. Lett. B **491**, 219 (2000).
 - [10] C. J. Batty, E. Friedman, and A. Gal, Nucl. Phys. A. **689**, 721 (2001).
 - [11] E. Friedman, Nucl. Phys. A **925**, 141 (2014); Hyperfine Interact. **234**, 77 (2015).
 - [12] T. G. Lee and C. Y. Wong, Phys. Rev. C **89**, 054601 (2014).
 - [13] T. G. Lee and C. Y. Wong, Phys. Rev. C **93**, 014616 (2016).
 - [14] T. G. Lee, C. Y. Wong, and L. S. Wang, Chin. Phys. **17** 2897 (2008); C. Y. Wong and T. G. Lee, Ann. Phys. **326**, 2138 (2011).
 - [15] T. Bressani and A. Filippi, Phys. Rep. **383** 213 (2003).
 - [16] C. Barbina *et al.*, Nucl. Phys. A **612**, 346 (1997).
 - [17] M. Astrua, *et al.*, Nucl. Phys. A **697**, 209 (2002).
 - [18] K. V. Protasov, V. Gudkov, E. A. Kupriyanova, V. V. Nesvizhevsky, W. M. Snow, and A. Yu. Voronin., Phys. Rev. D., **102**, 075025 (2020).
 - [19] V. V. Nesvizhevsky, V. Gudkov, K. V. Protasov, W. M. Snow, and A. Yu. Voronin., Phys. Rev. Lett., **122**, 221802 (2019).
 - [20] E. S. Golubeva, J. L. Barrow, and C. G. Ladd, Phys. Rev. D., **99**, 035002 (2019)
 - [21] D. G. Phillips *et al.*, Physics Reports **612**, 1 (2016).
 - [22] C. B. Dover, A. Gal, and J. M. Richard, Phys. Rev. D **27**, 1090 (1983); Phys. Rev. C **31**, 1423 (1985); Nucl. Instrum. Methods Phys. Res., Sect. A **284**, 13 (1989).
 - [23] L. A. Kondratyuk., JETP. Lett. **64**, 495 (1996).
 - [24] E. Friedman and A. Gal., Phys. Rev. D **78**, 016002 (2008).
 - [25] L. D. Landau and E. M. Lifshitz, *Quantum Mechanics* (Pergamon, Oxford 1958).
 - [26] T. G. Lee and C. Y. Wong, Phys. Rev. C **97**, 054617 (2018).
 - [27] ECIS97 (<https://people.nsl.msu.edu/~brown/reaction-codes/home.html>); J. Raynal., Phys. Rev. C., **23**, 2571 (1981)
 - [28] C. Ramsauer, Ann. Phys., **66**, 546 (1921).
 - [29] J. M. Peterson, Phys. Rev. **125**, 955 (1962).
 - [30] H. Marshak, A. Langford, C. Y. Wong, and T. Tamura, Phys. Rev. Lett., **20**, 554 (1968); H. Marshak, A. Langford, T. Tamura and C. Y. Wong, Phys. Rev. C **5**, 1862 (1970).
 - [31] H. Esbensen, Phys. Rev. C **85**, 064611 (2012).
 - [32] C. Y. Wong, Phys. Rev. C **86**, 064603 (2012).
 - [33] N. Rowley and K. Hagino, Phys. Rev. C **91**, 044617 (2015).
 - [34] K. W. Ford and J. A. Wheeler, Ann. Phys., **7**, 239 (1959); **7**, 259 (1959).
 - [35] M. V. Berry and K. L. Mount, Rep. Prog. Phys. **35** 315 (1972).
 - [36] W. H. Miller, Adv. Chem. Phys. **25**, 69 (1974).
 - [37] D. M. Brink and N. Takigawa, Nuc. Phys. A **279** 159 (1977).
 - [38] S. Y. Lee, N. Takigawa, and C. Marty, Nuc. Phys. A **308** 161 (1978).
 - [39] S. Ohkubo and D. M. Brink, Phys. Rev. C **36**, 966 (1987).
 - [40] P. H. Bowen, J. P. Scanlon, G. H. Stafford, J. J. Thresher, P. E. Hodgson., Nucl. Phys. **22**, 640 (1961).
 - [41] J. M. Blatt and V. F. Weisskopf, *Theoretical Nuclear Physics*, John Wiley and Sons, N.Y., 1952, p. 324.

[42] N. T. Zhang *et al.*, Physics Letters B, **801**, 135170 (2020).